

18. J. Urquidi, S. Singh, C. H. Cho, G. W. Robinson, *Phys. Rev. Lett.* **83**, 2348 (1999).
19. A. K. Soper, M. A. Ricci, *Phys. Rev. Lett.* **84**, 2881 (2000).
20. W. Utsumi *et al.*, *J. Phys.: Condens. Matter* **14**, 10497 (2002).
21. A cube made of boron and epoxy mixture was used as a pressure-transmitting medium. The temperature was monitored by a thermocouple and at high temperatures, when it broke, the temperature was estimated by the applied heater power. The error in the temperature determination is $\pm 50^\circ\text{C}$. The pressure was determined by x-ray diffraction measurements on boron nitride using a reported equation of state (28). The error in the pressure determination is about ± 0.2 GPa.
22. K. Funakoshi, A. Suzuki, H. Terasaki, *J. Phys.: Condens. Matter* **14**, 11343 (2002).
23. E. Hutchinson, *Trans. Faraday Soc.* **39**, 229 (1943).
24. V. V. Brazhkin, R. N. Voloshin, S. V. Popova, A. G. Lyapin, in *New Kinds of Phase Transitions: Transformations in Disordered Substances*, V. V. Brazhkin, S. V. Buldyrev, V. N. Ryzhov, H. E. Stanley, Eds. (Kluwer, Dordrecht, Netherlands, 2002), pp. 239–254.
25. Y. Katayama *et al.*, *J. Synchrotron Radiat.* **5**, 1023 (1998).
26. S. Endo, Y. Akahama, S. Terada, S. Narita, *Jpn. J. Appl. Phys.* **21**, L482 (1982).
27. The density was obtained from curve fit for the absorption profile in Fig. 3 using the following formulas: $\frac{I}{I_0} = C \int_{\text{beam}} \exp(-\mu_1 \rho_1 t_1 - \mu_2 \rho_2 t_2) dx dy$, $t_1(x) = 2\sqrt{r_1^2 - (x - x_{0,1})^2}$, $t_2(x) = 2\sqrt{r_2^2 - (x - x_{0,2})^2} - t_1$. Here, I/I_0 is a ratio of incident and transmitted x-ray intensities, C is a constant, μ_i is the x-ray mass absorption coefficient, ρ_i is the density, r_i is the radius, x is the horizontal position, y is the vertical position, and $x_{0,i}$ is the center position. Suffix 1 and 2 indicate sample and sapphire, respectively. We measured the x-ray diffraction and x-ray absorption of the black phosphorus sample before melting. From the lattice constant and absorption profile, μ_1 was experimentally determined. The product $\mu_2 \rho_2$ was chosen to reproduce the absorption profile of sapphire ring and was fixed. Radii r_1 and r_2 were fixed to 0.5 and 1.0 mm, respectively.
28. Y. Le Godec *et al.*, *High Pressure Res.* **17**, 35 (2000).
29. We thank K. Tsuji, M. Yao, Y. Akahama, T. Morishita, Y. Senda, K. Hoshino, V. V. Brazhkin, and K. Funakoshi for their helpful discussions. We thank Y. Akahama for supplying black P sample. We also thank the staffs of JAERI and Spring-8 for their technical supports.

13 July 2004; accepted 22 September 2004

Energetics of Hydrogen Bond Network Rearrangements in Liquid Water

Jared D. Smith, Christopher D. Cappa, Kevin R. Wilson, Benjamin M. Messer, Ronald C. Cohen, Richard J. Saykally*

A strong temperature dependence of oxygen K-edge x-ray absorption fine structure features was observed for supercooled and normal liquid water droplets prepared from the breakup of a liquid microjet. Analysis of the data over the temperature range 251 to 288 kelvin (-22° to $+15^\circ\text{C}$) yields a value of 1.5 ± 0.5 kilocalories per mole for the average thermal energy required to effect an observable rearrangement between the fully coordinated (“ice-like”) and distorted (“broken-donor”) local hydrogen-bonding configurations responsible for the pre-edge and post-edge features, respectively. This energy equals the latent heat of melting of ice with hexagonal symmetry (ice Ih) and is consistent with the distribution of hydrogen bond strengths obtained for the “overstructured” ST2 model of water.

A detailed description of the hydrogen bond (H bond) network in liquid water is the key to understanding its unusual properties. The combined results of x-ray and neutron scattering experiments, thermodynamics data, and classical as well as ab initio molecular dynamics (MD) simulations have long been interpreted in terms of a locally tetrahedral liquid structure, wherein (on average) each water molecule is H-bonded to four nearest neighbors via two donor bonds and two acceptor bonds. This view was recently challenged by Wernet *et al.* (1), who used state-of-the-art x-ray Raman and absorption spectroscopy in conjunction with density functional theory (DFT) calculations to deduce the structure of the first coordination shell in liquid water. From their analysis, they contend that room-temperature liquid water instead comprises a large fraction ($>80\%$) of broken H bonds and that, on average, each molecule only forms

two strong H bonds: one acceptor and one donor. Such a structure implies that liquid water comprises primarily rings or chains, a stark contrast to the traditional perspective.

Specifying the average number of H bonds formed per molecule is straightforward when dealing with computer simulations of water, given specific (albeit necessarily arbitrary) energetic (2–5) or geometric (6–8) criteria for defining an H bond. The choice of an energetic H-bond criterion is often based on the form of the intermolecular bonding energy distribution obtained from simulations (2, 3), or else an energetic cutoff is chosen such that the overwhelming majority of molecules form four or fewer H bonds (4, 5). The resulting H-bond statistics are, of course, highly dependent on the precise definition used.

Experimental measurements, however, necessarily define H bonds in terms of the particular experimental technique used (9). In recent years, several new experiments have been reported that use x-ray absorption spectroscopy (XAS) and x-ray Raman spectroscopy (XRS) to characterize the H-bonding

environment in liquid water by assigning the observed spectral features near the O(1s) ionization edge to specific H-bonding configurations (1, 7, 10–15). In particular, the intensity in the pre-edge region (~ 535 eV) is assigned to water molecules with a broken or distorted H-bond on the donor side, whereas the post-edge feature (~ 541 eV) has been identified with molecules having four strong and highly symmetric H bonds, as in ice Ih. Here, we report an experimentally determined energetic criterion characterizing the degree of H-bond distortion required to effect observable spectral changes in the pre-edge and post-edge intensities measured in the total electron yield near-edge x-ray absorption fine structure (TEY-NEXAFS) spectrum of liquid water as a function of temperature. We show that pre-edge intensity arises from relatively small distortions of an “ice-like” H bond, and that considerable intensity found in the pre-edge region can be expected even for nearly perfect tetrahedral configurations.

We recorded TEY-NEXAFS spectra for supercooled and normal water from 251 to 288 K (1 atm) by using a liquid microjet to control the temperature. The details of our experimental techniques were previously described (14, 16). Two area-normalized spectra (Fig. 1) recorded at 288 and 254 K show that there is a clear increase in pre-edge intensity with increasing temperature. Furthermore, the conduction band between 537 and 545 eV broadens and becomes reduced in intensity with increasing temperature. We decomposed the spectra into six Gaussian subbands, one for each feature found in the gas-phase NEXAFS spectrum (Fig. 1). Variations in the subbands centered at the post-edge and pre-edge are almost exclusively responsible for the observed spectral changes. The pre-edge region shows a 20 to 25% increase in intensity over the 37 K range studied, whereas the post-edge intensity shows a corresponding 12 to 18% decrease. This result is consistent with the observation that the pre-edge intensity arises from molecules with broken or distorted H bonds,

Department of Chemistry, University of California, Berkeley, CA 94720, USA.

*To whom correspondence should be addressed. E-mail: saykally@berkeley.edu

whereas the post-edge intensity arises from fully coordinated and highly symmetric species. These large changes in intensity are a striking contrast to the minor changes observed in the pair correlation function over the same temperature range (17), indicating that the x-ray absorption spectrum is particularly sensitive to small changes in the H-bond structure.

If we assume that the pre-edge (I_{pre}) and post-edge (I_{post}) intensities arise from molecules in two general classes of H-bonding configurations (distorted or “broken-donor” bonds and fully coordinated ice-like bonds, respectively), for which relative populations are a function of absolute temperature T only, a plot of $\ln(I_{\text{pre}}/I_{\text{post}})$ versus $1/T$ will yield a straight line with a slope that is proportional to the average difference in energy between the two classes (ΔE). A linear fit to the data yields a correlation coefficient of 0.98 and a slope of $\Delta E/R$, where R is the universal gas constant, that gives the rearrangement energy between the two classes of H-bonding distributions as 1.5 ± 0.5 kcal/mol (Fig. 2) (18–20). This concept of thermally activated H-bond breakage follows the discussion given by Stillinger regarding the isosbestic point in the distribution of H-bond energies from the ST2 potential (2).

The average energy of a fully formed ice-like H bond, such as those that generate

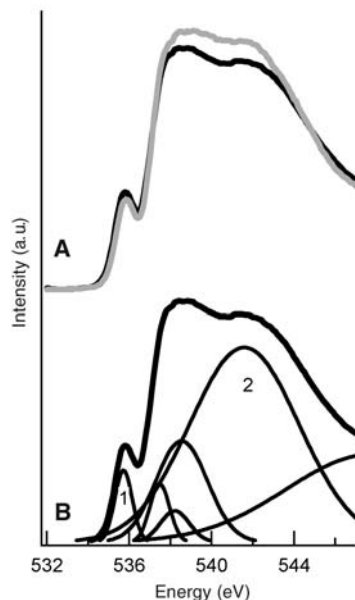


Fig. 1. (A) Comparison of the TEY-NEXAFS taken at two different temperatures. The solid black curve was recorded at 288 K and the gray curve at 254 K. (B) A TEY-NEXAFS spectrum taken at 288 K (bold curve) showing the Gaussian subbands used to deconvolute specific components of the spectrum. The subbands labeled 1 and 2, centered at the pre-edge and post-edge regions, respectively, are the only regions to exhibit temperature dependence.

the post-edge feature, is about -5.5 kcal/mol (2, 21). Therefore, the difference in energy (1.5 kcal/mol) between the two H-bonding distributions results from the loss of $27 \pm 9\%$ of the average H-bond energy. Wernet *et al.* (1) deduced that the presence of a pre-edge peak corresponds to the loss of $55 \pm 15\%$ of the H-bonding energy. The XAS H-bonding criteria reported by Wernet *et al.* were established by carefully exploring angular and radial distortions on both the acceptor and donor H bonds of the central molecule in a computer-generated ice-like 11-molecule cluster; the computed XAS spectra that had a distinct pre-edge feature were associated with broken-donor H bonds. However, the rigid ice-like model cluster and the small number of configurations considered in that study may not adequately represent liquid water and may have thus led to an unphysical value of this critical parameter.

Given that our ΔE constitutes the definition of the energy required to measurably distort an H bond in an XAS experiment, the more permissive criteria derived by Wernet *et al.* (1) can easily account for the discrepancy between the controversial H-bond structure they proposed and the textbook description of local tetrahedral structure. It is instructive to compare the number of H bonds per water molecule calculated from MD simulations using different energetic criteria. Blumberg *et al.* (22) made such a comparison for an ST2 simulation at 284 K. Using a lower limit of -4 kcal/mol for the H-bond energy, they found an average value of 2.2 hydrogen bonds per molecule

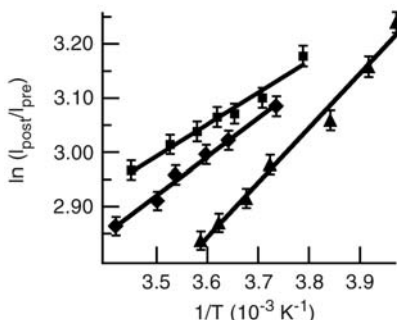


Fig. 2. Plots of the natural logarithm of the post-edge and pre-edge subband area ratio versus inverse temperature, taken from three separate experiments. The error bars represent twice the SD in the Gaussian fits (Fig. 1). The solid lines represent linear fits ($R^2 \geq 0.98$) with a slope of $\Delta E/R$. ΔE , the difference in energy between the two different H-bonding distributions, is determined to be 1.5 ± 0.5 kcal/mol. The microjet diameters used in these experiments were 30 μm (\blacksquare and \blacklozenge) and 7.6 μm (\blacktriangle). Although each experiment is self-consistent, changes in the collection geometry, beamline calibration, and baseline cause variations in the measured slope and intercept of the fitted line. Therefore, the ΔE reported here is the average of the three independent measurements shown (\pm SD).

(23). This energy cutoff is equivalent to the experimental x-ray absorption criterion determined here, assuming that the ice-like post-edge species has an average H-bond energy of -5.5 kcal/mol (2, 21) and given that the distorted broken-donor distribution responsible for the pre-edge feature lies 1.5 kcal/mol higher in energy. The low number of H bonds per molecule calculated from this cutoff does not suggest that ST2 water lacks local tetrahedral structure; rather, it underscores the sensitivity of this parameter to the exact definition of a hydrogen bond that is used to compute it. Furthermore, using the lower H-bond energy limit of Wernet *et al.* (~ 2.5 kcal/mol) (1), we calculate the average number of H bonds to be 3.3.

The ST2 effective pair potential (24) predicts an excessively tetrahedral structure when compared with experimental radial distribution functions (25). Thus, using the criterion for what constitutes a distorted H bond as determined by an x-ray absorption experiment, the large population of broken-donor bonds found by Wernet *et al.* (1) is actually in good agreement with the local tetrahedral structure predicted by “overstructured” MD simulations, again reflecting the fact that the x-ray experiment is highly sensitive to even very small distortions of the H bond. This conclusion is consistent with recent results by Hetenyi *et al.* (7) in which the NEXAFS spectrum was calculated from an ab initio simulation of 64 water molecules. The resulting spectrum from the tetrahedrally structured simulation is in qualitative agreement with experimental NEXAFS spectra of water.

We note that the value of this energy difference (1.5 ± 0.5 kcal/mol) between the symmetric ice-like and broken-donor H bond distributions equals, to within experimental accuracy, the latent heat of melting of ice Ih (1.4 kcal/mol). We have recently carried out a study of the temperature dependence of the water Raman spectrum, treated previously by Walrafen (20), which yields a similar result (1.4 ± 0.2 kcal/mol) (16). Moreover, the peak of the librational band in the Raman spectrum of liquid water (the hindered rotation of water molecules) also occurs near this energy (20), and this librational motion is precisely that which most effectively “breaks” a hydrogen bond. Hence, it may be possible to view 1.5 kcal/mol as the average energy required to “break” a hydrogen bond in a locally symmetric, strongly H-bonded (ice-like) domain in both solid and liquid water.

References and Notes

1. Ph. Wernet *et al.*, *Science* **304**, 995 (2004).
2. F. H. Stillinger, *Science* **209**, 451 (1980).
3. W. L. Jorgensen *et al.*, *J. Chem. Phys.* **79**, 926 (1983).
4. A. Geiger, H. E. Stanley, *Phys. Rev. Lett.* **49**, 1749 (1982).
5. H. E. Stanley, J. Teixeira, *J. Chem. Phys.* **73**, 3404 (1980).
6. I. W. Kuo, C. J. Mundy, *Science* **303**, 658 (2004).

7. B. Hetenyi, F. De Angelis, P. Giannozzi, R. Car, *J. Chem. Phys.* **120**, 8632 (2004).
8. A. Luzar, D. Chandler, *J. Chem. Phys.* **98**, 8160 (1993).
9. G. A. Jeffrey, *Introduction to Hydrogen Bonding* (Oxford Univ. Press, New York, 1997), pp. 11–12.
10. K. R. Wilson *et al.*, *J. Phys. Condens. Matter* **14**, L221 (2002).
11. S. Myneri *et al.*, *J. Phys. Condens. Matter* **14**, L213 (2002).
12. H. Bluhm *et al.*, *J. Phys. Condens. Matter* **14**, L227 (2002).
13. J.-H. Guo *et al.*, *Phys. Rev. Lett.* **89**, 137402 (2002).
14. K. R. Wilson *et al.*, *Rev. Sci. Instrum.* **75**, 725 (2004).
15. U. Bergmann *et al.*, *Phys. Rev. B* **66**, 092107 (2002).
16. See supporting data on Science Online.
17. R. Corban, M. D. Zeidler, *Ber. Bunsenges. Phys. Chem.* **96**, 1463 (1992).
18. We caution that this method for determining ΔE could imply an oversimplification of the actual spectrum. We have assumed that the pre-edge intensity arises exclusively from molecules with one or two broken-donor H bonds, whereas the post-edge intensity is a result of fully coordinated species. Under this assumption, the pre-edge intensity can be expressed as

$$I_{\text{pre}} \propto \sigma_{\text{pre}} \exp(-E_{\text{pre}}/RT)$$

where σ_{pre} is the cross section at 535 eV for the broken-donor bond configurations, and E_{pre} is the average energy of molecules in these configurations. A similar expression can be written for the post-edge intensity, and the ratio of intensities can then be written as

$$\ln(I_{\text{post}}/I_{\text{pre}}) = -\Delta E/RT + \ln(a)$$

where a is a constant with respect to temperature. If other H-bonding configurations also produce appreciable absorption in these regions, we would expect deviations from linearity. Therefore, the quality of the linear fit evident in Fig. 2 is an indication that this simple model is appropriate, at least as a first approximation. This type of analysis is similar to that used to interpret the temperature-dependent Raman spectrum of liquid water (19, 20).

19. D. E. Hare, C. M. Sorenson, *J. Chem. Phys.* **93**, 6954 (1990).
20. G. E. Walrafen, in *Water: A Comprehensive Treatise*, F. Franks, Ed. (Plenum, New York, 1972), vol. 1.
21. S. J. Suresh, V. M. Naik, *J. Chem. Phys.* **113**, 9727 (2000).
22. R. L. Blumberg *et al.*, *J. Chem. Phys.* **80**, 5230 (1984).
23. The energetic cutoff is defined such that two molecules are considered H-bonded to one another only if the computed pair potential is less than -4 kcal/mol. Furthermore, if any molecule has more than four H

bonds according to the cutoff, only the four strongest bonds are considered.

24. F. H. Stillinger, A. Rahman, *J. Chem. Phys.* **60**, 1545 (1974).
25. J. M. Sorenson *et al.*, *J. Chem. Phys.* **113**, 9149 (2000).
26. Supported by the National Defense Science and Engineering Graduate Fellowship Program (C.D.C.) and by the Chemical Sciences Division of the U.S. Department of Energy. This research was carried out at the Advanced Light Source (ALS) beamline 8.0.1, Lawrence Berkeley National Laboratory. The Advanced Light Source is supported by the Office of Basic Energy Sciences, Materials Sciences Division, of the U.S. Department of Energy under contract DE-AC03-76SF0098 at Lawrence Berkeley National Laboratory. We thank the ALS staff, including M. Gilles, B. Rude, and J. Denlinger, for assistance.

Supporting Online Material

www.sciencemag.org/cgi/content/full/306/5697/851/DC1

Materials and Methods

Figs. S1 and S2

References

9 July 2004; accepted 23 September 2004

Probabilistic Tomography Maps Chemical Heterogeneities Throughout the Lower Mantle

Jeannot Trampert,^{1*} Frédéric Deschamps,¹
Joseph Resovsky,¹ Dave Yuen²

We obtained likelihoods in the lower mantle for long-wavelength models of bulk sound and shear wave speed, density, and boundary topography, compatible with gravity constraints, from normal mode splitting functions and surface wave data. Taking into account the large uncertainties in Earth's thermodynamic reference state and the published range of mineral physics data, we converted the tomographic likelihoods into probability density functions for temperature, perovskite, and iron variations. Temperature and composition can be separated, showing that chemical variations contribute to the overall buoyancy and are dominant in the lower 1000 kilometers of the mantle.

To understand the nature of mantle convection, it is essential to quantify thermal and compositional contributions to the density variations that drive the solid-state flow. Although seismic tomography is probably the best probe for Earth's three-dimensional structure, its main constraint is on wave speeds rather than density. It has therefore been common practice in tomography to prescribe a scaling between density and velocity variations (I) and invert for velocity only. Such a scaling is justified if a single cause is responsible for the observed varia-

tions. Temperature-induced ratios of relative density to relative shear wave speed variations between 0.2 to 0.4 have been measured (2, 3) and are compatible with geodynamic data, combined with specific viscosity profiles (4, 5). This, together with evidence from seismology that slabs penetrate deep into the mantle (6, 7), led to the view that mantle dynamics is dominated by thermally driven whole-mantle convection (8). Chemical buoyancy (9) was introduced mainly to explore the possible thermochemical nature of D'' in terms of a primordial layer (10–14), subducted oceanic crust (14–16), or chemical reactions with the core (17). These Boussinesq calculations, however, are not realistic, because the simulated high-density contrasts are not compatible with the observed seismic velocities and a plausible mineralogic model (18). When an extended Boussinesq or compressible calculation is used, the re-

quired density contrasts are reduced (19–21). More interestingly, in models where thermal expansivity decreases with depth, thermochemical superplumes are seen to develop (20–22), not unlike those found under Africa and the Pacific in tomography (23, 24). With improving resolution of seismic velocities and, especially, of density, indirect evidence has emerged suggesting that compositional heterogeneity is present in the lower mantle (5, 25–32). In an effort to reconcile evidence from various research fields, dynamical models with a strong compositional component (33–35) have challenged the classic view of thermally driven mantle convection.

Owing to trade-offs between temperature and composition, wave speeds alone are not sufficient to infer their variations, and density constraints should be included (5, 31, 36). Normal modes require weak and/or negative correlations between density and shear wave speed variations throughout most of the lower mantle (28), but amplitudes of density are difficult to infer (37). We represent the seismic constraints with more complete likelihoods, rather than individual models, and have extended the work of Resovsky and Trampert (32) to spherical harmonic degree 6 for relative variations of bulk sound ($d\ln V_p$) and shear wave speed ($d\ln V_s$), density ($d\ln \rho$), and topography at the 670-km discontinuity and at the core-mantle boundary (CMB). In addition to providing a full uncertainty analysis (errors and trade-offs), representing the data as likelihoods of seismic parameters allows a subsequent incorporation of additional data constraints. Most often, geodynamic data are jointly inverted with the seismologic data (5, 28), but in our approach, it is more efficient to filter a posteriori the purely seismic models by retaining only those that fit the gravity field within

¹Department of Earth Sciences, Utrecht University, Post Office Box 80021, 3508 TA Utrecht, Netherlands. ²Minnesota Supercomputer Institute, Department of Geophysics University of Minnesota, Minneapolis, MN 55455–0219, USA.

*To whom correspondence should be addressed. E-mail: jeannot@geo.uu.nl